PAPER • OPEN ACCESS

The phase-space structure of a nonlinear ion diffusion tensor in ion-temperature-gradient-driven turbulence

To cite this article: Shiqiao Sun *et al* 2023 *Nucl. Fusion* **63** 086030

OPEN ACCESS
IOP Publishing | International Atomic Energy Agency
Nuclear Fusion
Nucl. Fusion **63** (2023) 086030 (12pp)
https://doi.org/10.1088/1741-4326/ace2d5

The phase-space structure of a nonlinear ion diffusion tensor in ion-temperature-gradient-driven turbulence

Shiqiao Sun[1], **Yuesong Li**[1], **Zihao Wang** and **Shaojie Wang***

School of Physical Science, University of Science and Technology of China, Hefei 230026, China

E-mail: wangsj@ustc.edu.cn

Received 15 January 2023, revised 4 June 2023
Accepted for publication 29 June 2023
Published 12 July 2023

Abstract

The phase-space structure of an ion diffusion tensor in ion temperature gradient (ITG)-driven turbulence is studied using the newly developed numerical code Numerical Diagnosis of Transport Matrix. The numerical results show that at both the linear and nonlinear stage, the diffusion tensor of ITG turbulence presents a typical ballooning structure in the poloidal direction and a magnetic drift resonance structure in velocity space. The D^{rr} and D^{rK} components of the diffusion tensor satisfy the Stokes–Einstein relation. It is found that the phase-space structure of the ion diffusion tensor at the linear stage is induced by the resonance between ions and ITG eigenmodes, while that at the nonlinear stage is induced by the resonance between ions and the daughter ballooning modes under the poloidal acceleration of nonlinear zonal radial electric fields.

Keywords: ITG turbulence, phase-space structure, nonlinear diffusion tensor, nonlinear resonance, gyrokinetic simulation

(Some figures may appear in colour only in the online journal)

1. Introduction

The anomalous transport induced by plasma turbulence plays an important role in the evolution of magnetically confined plasma. Understanding the mechanism and characteristics of anomalous turbulent transport is one of the most important issues in fusion plasma physics. The transport in plasma can be understood as the phase-space convection and diffusion effect [1]. In classical [2] and neo-classical [3] transport, the diffusion is induced by Coulomb collisions between particles; in anomalous transport, the diffusion is considered as the result of the interaction between particles and turbulence [4]. In transport theories, the diffusion effect can be described by the diffusion tensor [5, 6]. The phase-space structure of the diffusion tensor is very important in understanding the anomalous transport phenomena since it determines the macroscopic transport matrix and, consequently, the driving effects of thermodynamic general forces on the transport fluxes. For example, it is found that the strong ballooning poloidal structure of an ion diffusion tensor could lead to inward toroidal angular momentum flux driven by magnetic field curvature [7, 8], which may play an important role in the generation of plasma intrinsic rotation [9]; it is also found that the magnetic-drift-resonance-induced velocity structure of an ion diffusion tensor

[1] These authors contribute equally to this paper.
[*] Author to whom any correspondence should be addressed.

could lead to inward ion heat flux driven by parallel flow [10], which may explain the anomalous reduction in ion thermal diffusivities observed in the TFTR [11] and JT-60U [12].

At present, the quasilinear theory is the most commonly used method to estimate the phase-space structure of a diffusion tensor, either for explaining the experimental observation [13, 14] or calculating the macroscopic transport coefficient used in the integrated modeling of tokamak plasmas [15]. The quasilinear theory is suitable for investigation of the turbulent diffusion in the linear stage of turbulence with low amplitude, during which the nonlinear effects are negligible. However, when the turbulence evolves to the saturation stage, the nonlinear effects become important, and thus the quasilinear theory is not applicable in this situation in principle [16]. Therefore, the characteristics of the phase-space structure of the diffusion tensor in different types of fully developed plasma turbulence are still open issues.

Based on the nonlinear phase-space Fokker–Planck equation [17], a diagnostic code, the Numerical Diagnosis of Transport Matrix (NDTM), has been developed recently [18], which could obtain the nonlinear ion phase-space diffusion tensor and macroscopic transport matrix from the gyrocenter orbits in the turbulent field found by the nonlinear gyrokinetic simulations. In a previous publication [18], we have reported the numerical results of the nonlinear ion transport matrix in ion temperature gradient (ITG)-driven turbulence obtained by the NDTM code, but the results of the phase-space ion diffusion tensor have not been discussed. In this paper, we report the phase-space structure of a nonlinear ion diffusion tensor in ITG turbulence obtained by the NDTM code, and a ballooning structure in the poloidal direction and a magnetic-drift-resonance structure in velocity space have been observed. To understand the results, we further investigate the ion diffusion tensor structure in single-n ITG modes (here, n is the toroidal mode number). We find that the resonance structures observed are generated by the resonance of ions and ITG turbulence under the influence of zonal flows.

The remaining part of this paper is organized as follows: in section 2, we introduce the fundamentals of the NDTM code; in section 3, we show the numerical results of the phase-space structure of the nonlinear ion diffusion tensor in ITG turbulence; in section 4, we show the ion diffusion tensor structure in single-n toroidal Fourier modes; in section 5, the main results are summarized.

2. The fundamentals

The collisionless plasma can be described by the nonlinear Vlasov equation

$$\partial_t f(\boldsymbol{Z},t)+\partial_{\boldsymbol{Z}}\cdot[\dot{\boldsymbol{\mathcal{Z}}}(\boldsymbol{Z},t)f]=0, \tag{1}$$

where f is the distribution function, $\boldsymbol{Z}$ is the phase-space coordinate, and t is the time. Based on the stationary–homogeneous assumption of the plasma turbulence, the nonlinear phase-space Fokker–Planck transport equation in convection–diffusion form can be derived from equation (1) [17],

$$\partial_t F(\boldsymbol{Z},t)+\partial_{\boldsymbol{Z}}\cdot\left[\left\langle\dot{\boldsymbol{\mathcal{Z}}}\right\rangle F(\boldsymbol{Z},t)-\boldsymbol{D}\cdot\partial_{\boldsymbol{Z}}F(\boldsymbol{Z},t)\right]=0, \tag{2}$$

where $F(\boldsymbol{Z},t)\equiv\langle f(\boldsymbol{Z},t)\rangle=\frac{1}{T}\int_{t-\frac{T}{2}}^{t+\frac{T}{2}}f(\boldsymbol{Z},t')\mathrm{d}_E t'$ is the ensemble-averaged distribution function, and $\boldsymbol{D}(\boldsymbol{Z},t)$ is the ion phase-space diffusion tensor

$$\boldsymbol{D}(\boldsymbol{Z},t)=\frac{1}{2T}\int_{t-\frac{T}{2}}^{t+\frac{T}{2}}\mathrm{d}_E t'\,\dot{\boldsymbol{\mathcal{Z}}}(\boldsymbol{Z},t')\int_{t-\frac{T}{2}}^{t+\frac{T}{2}}\mathrm{d}_L t''\,\dot{\boldsymbol{\mathcal{Z}}}[\boldsymbol{\mathcal{Z}}(t'';\boldsymbol{Z},t'),t''], \tag{3}$$

where T represents the ensemble-average time; $\boldsymbol{\mathcal{Z}}(t'';\boldsymbol{Z},t')$ denotes the phase-space coordinate at time t'' of a particle, which passes through $\boldsymbol{Z}$ at time t'; $\mathrm{d}_E t'$ denotes the Eulerian time integral, which means Z in the kernel should be understood as a constant; and $\mathrm{d}_L t''$ denotes the Lagrangian time integral, which means the integral path should be along the particle orbit. It can be seen that the phase-space ion diffusion tensor is determined by the particle orbit in turbulence. In the electrostatic turbulence with low frequency, the particle orbit can be described by the gyrocenter Hamiltonian equation

$$\dot{\boldsymbol{\mathcal{Z}}}(\boldsymbol{Z},t)=\{\boldsymbol{Z},H_0(\boldsymbol{Z})+e_s\langle\delta\phi\rangle_{\mathrm{gyro}}(\boldsymbol{X},\mu,t)\}, \tag{4}$$

where e_s is the particle charge, $H_0(\boldsymbol{Z})$ is the unperturbed Hamiltonian, $\{,\}$ is the Poisson bracket, and $\langle\delta\phi\rangle_{\mathrm{gyro}}(\boldsymbol{X},\mu,t)$ is the gyro-averaged turbulence electrostatic potential obtained from the simulation data. Here, $\boldsymbol{Z}=(\boldsymbol{X},v_\parallel,\mu)$ is the five-dimensional gyrocenter coordinate, where $\boldsymbol{X}$ is the gyrocenter position, $v_\parallel$ is the parallel velocity, and μ is the magnetic momentum. Note that equation (4) should be integrated along the real orbit. The formula for the phase-space ion diffusion tensor is illustrated in figure 1.

It should be pointed out that the phase-space ion diffusion tensor $\boldsymbol{D}$ should be toroidally symmetric in a tokamak configuration. In practical computation, $\boldsymbol{D}$ is the function of $(\boldsymbol{X},v_\parallel,\mu,t)$. To ensure the exact recovery of toroidal symmetry, the phase-space ion diffusion tensor $\boldsymbol{D}$ is toroidally averaged, which is carried out in practice by taking the average over 80 uniform toroidal grid points in our simulation.

The phase-space ion diffusion tensor includes multiple components, in which the transport in ITG turbulence is mainly determined by the properties of the D^{rr} and D^{rK} components. Following equation (3), one can write the D^{rr} and D^{rK} components immediately,

$$D^{rr}(\boldsymbol{Z},t)=\frac{1}{2T}\int_{t-\frac{T}{2}}^{t+\frac{T}{2}}\mathrm{d}_E t'\,\dot{r}(\boldsymbol{Z},t')\times\int_{t-\frac{T}{2}}^{t+\frac{T}{2}}\mathrm{d}_L t''\,\dot{r}[\boldsymbol{\mathcal{Z}}(t'';\boldsymbol{Z},t'),t''], \tag{5a}$$

$$D^{rK}(\boldsymbol{Z},t)=\frac{1}{2T}\int_{t-\frac{T}{2}}^{t+\frac{T}{2}}\mathrm{d}_E t'\,\dot{r}(\boldsymbol{Z},t')\times\int_{t-\frac{T}{2}}^{t+\frac{T}{2}}\mathrm{d}_L t''\,\dot{K}[\boldsymbol{\mathcal{Z}}(t'';\boldsymbol{Z},t'),t''], \tag{5b}$$

where $K=\frac{1}{2}m_{\mathrm{i}}v_\parallel^2+\mu B$ is the gyrocenter energy, m_{i} is the ion mass, and B is the magnetic field. Note that equations (5a)

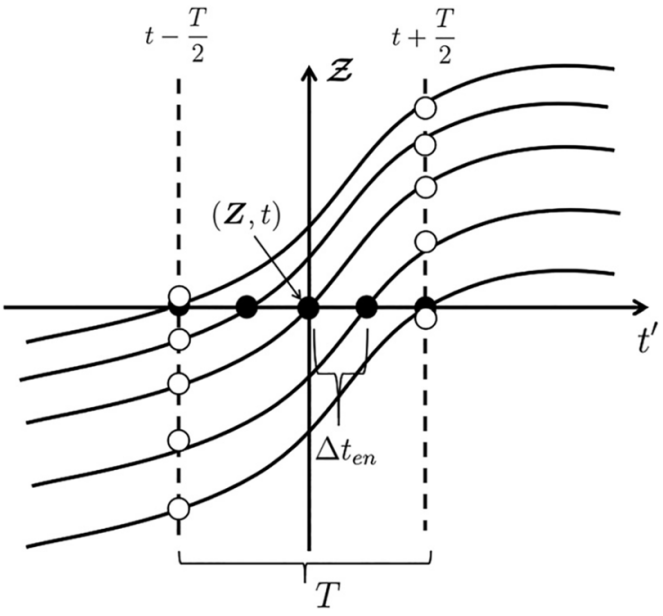

Figure 1. An illustration of the formula of the ion phase-space diffusion tensor. Black curves denote different particle orbits. Black points denote the points with the same phase-space position $\boldsymbol{Z}$ but different time t', while white points denote different phase-space positions $\boldsymbol{Z}$ but the same time $t\pm\frac{T}{2}$. Each orbit can be calculated by integrating equation (4) from black points forward and backward to white points using the simulation data, $\langle\delta\phi\rangle_{\rm gyro}(\boldsymbol{X},\mu,t)$. Here, $\boldsymbol{D}(\boldsymbol{Z},t)$ is calculated by the gyrocenter velocity at the black points $\dot{\boldsymbol{\mathcal{Z}}}(\boldsymbol{Z},t')$ and the displacement of white points $\Delta\boldsymbol{\mathcal{Z}}(t;\boldsymbol{Z},t')=\boldsymbol{\mathcal{Z}}(t+\frac{T}{2};\boldsymbol{Z},t')-\boldsymbol{\mathcal{Z}}(t-\frac{T}{2};\boldsymbol{Z},t')$.

and (5*b*) are definitions of D^{rr} and D^{rK} in nonlinear theory, respectively.

In quasilinear theories, the ion diffusion tensor can be written as [6, 10]

$$\boldsymbol{D}_{\rm ql}=\partial_t\langle\boldsymbol{G}_1\boldsymbol{G}_1\rangle_\varepsilon, \tag{6}$$

with the generating vector given by

$$G_1^{\boldsymbol{X}}=-\frac{\boldsymbol{b}_0}{B_\parallel^*}\times\nabla S_1-\frac{\boldsymbol{B}^*}{B_\parallel^*}\frac{\partial S_1}{\partial v_\parallel}, \tag{7a}$$

$$G_1^{v_\parallel}=\frac{\boldsymbol{B}^*}{B_\parallel^*}\cdot\nabla S_1, \tag{7b}$$

the gauge function S_1 given by

$$\left(\frac{\mathrm{d}}{\mathrm{d}t}\right)_0 S_1=\langle\delta\phi\rangle_{\rm gyro}, \tag{8}$$

where $(\frac{\mathrm{d}}{\mathrm{d}t})_0$ denotes the derivative along the unperturbed orbit; the gauge function S_1 can be obtained by integrating the gyro-averaged turbulence electrostatic potential along the unperturbed orbit, in which the potential is considered as a linear eigenmode with constant frequency and growth rate.

It can be seen by comparing equations (3) and (6) that both the quasilinear and the nonlinear ion diffusion tensor reflect the response of the particle orbit to the turbulence field. Note that $G_1^{\boldsymbol{X}}, G_1^{v_\parallel}$ are the deviation of the gyrocenter from the unperturbed orbit. It should be pointed out that the essence of the quasilinear theory is that the deviation $(G_1^{\boldsymbol{X}},\ G_1^{v_\parallel})$ from the unperturbed orbit can be found perturbatively by integrating along the unperturbed orbit, since the perturbation is weak enough. However, when the perturbation is strong (in the nonlinear stage), the real orbit cannot be found by using a perturbation method; in this case, the deviation from the unperturbed orbit must be found by integrating the Hamiltonian equation along the real orbit.

Based on the nonlinear Fokker–Planck equation, we have developed the NDTM code. The NDTM code reads the nonlinear discrete time-dependent turbulent field simulated by a gyrokinetic turbulence code, evolves the nonlinear gyrocenter orbit in the turbulent field, and computes the ion diffusion tensor using equation (3). To validate the NDTM code, we have computed the macroscopic transport fluxes in ITG turbulence using the NDTM code; the results agree well with those obtained using the NLT code [18].

3. Phase-space structure of nonlinear ion diffusion tensor in ITG-driven turbulence

3.1. The numerical simulation of ITG turbulence

As in the previous work [18], the discrete ITG turbulent field used for the NDTM is simulated by the gyrokinetic turbulence code NLT. Based on the numerical Lie-transform method and the finite difference method, the NLT code solves the nonlinear gyrokinetic Vlasov equation [6, 19] and the gyrokinetic quasi-neutrality equation, respectively. The field-aligned coordinate is used [20] and, recently, the simulation domain includes the magnetic axis in the NLT [21]. Compared with the numerical results of other widely used global gyrokinetic codes, the linear and nonlinear NLT simulations of ITG instability have been verified [20, 22].

The Cyclone-base-case (Cbc) test parameter [23], with $R_0=1.67\,\mathrm{m}$, $a=0.6\,\mathrm{m}$, $B_0=1.9\,\mathrm{Tesla}$, is used, where R_0 and a are the major radius and minor radius of plasmas, respectively; B_0 is the magnetic field at the magnetic axis. The equilibrium temperature and density profile are set as

$$T_{\rm i}=T_{\rm e}\equiv T(r)=T_0\exp\left[-\kappa_T\frac{a}{R_0}\Delta_T\tanh\left(\frac{(r-r_0)/a}{\Delta_T}\right)\right],$$

$$N_{\rm i}=N_{\rm e}\equiv N(r)=N_0\exp\left[-\kappa_N\frac{a}{R_0}\Delta_N\tanh\left(\frac{(r-r_0)/a}{\Delta_N}\right)\right],$$

where $T_{\rm i}$ and $T_{\rm e}$ denote the ion and the electron temperature, respectively; $N_{\rm i}$ and $N_{\rm e}$ denote the ion and the electron density, respectively; $T_0=1.97\,\mathrm{keV}$, $N_0=10^{19}\,\mathrm{m}^{-3}$, $\kappa_T=6.96$, $\kappa_N=2.23$, $\Delta_T=\Delta_N=0.3$, $r_0=0.5a$. The ion charge is set as $e_{\rm i}=e$, where e is the elementary charge; the ion mass is set as $m_{\rm i}=2m_{\rm p}$, where $m_{\rm p}$ is the proton mass. The safety factor profile is set as

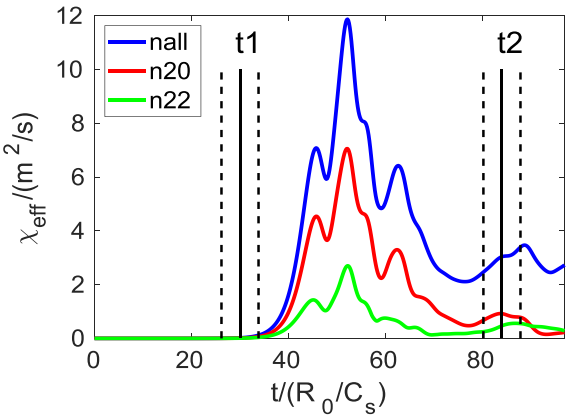

Figure 2. Effective heat diffusivity simulated by NLT. The quasilinear time t_1 and nonlinear time t_2 are labeled with black solid lines. The quasilinear time range $t_1 \pm \frac{T}{2}$ and nonlinear time range $t_2 \pm \frac{T}{2}$, the time integral domain in equation (3), are labeled with black dashed lines, where T is the interval for the time average. Here, nall means contribution from all the toroidal Fourier modes, and n20 and n22 mean contributions from the toroidal Fourier modes $n = 20$ and $n = 22$, respectively.

$$q(r) = 0.86 - 0.16\frac{r}{a} + 2.45\left(\frac{r}{a}\right)^2,$$

where r is the radial coordinate. The Coulomb collisions and external heating source are not considered in the simulation. The phase-space coordinate grid number is set as $N_r \times N_\theta \times N_\alpha \times N_{v_\parallel} \times N_\mu = 189 \times 16 \times 141 \times 64 \times 16$. A toroidal filter is applied to eliminate the perturbation with wave numbers higher than $N_\alpha/3$, and the system is considered symmetric in the toroidal direction with the period π; therefore, the toroidal Fourier modes with the number $n = 0, 2, \ldots, 40$ are kept in the simulation.

The effective heat diffusivity is shown in figure 2, which is defined as

$$\chi_{\rm eff}^{\rm NLT} = \frac{Q^r/n_i}{-\partial_r T_i} = \frac{\int \frac{1}{B^2}(-\nabla\langle\delta\phi\rangle_{\rm gyro} \times \boldsymbol{B})\cdot\nabla r\delta f K {\rm d}^3 v}{-n_i\partial_r T_i}. \quad (9)$$

The fluctuating electrostatic potential at t_1 and t_2, which will be used to compute the phase-space ion diffusion tensor at the corresponding times by using the NDTM code, is shown in figure 3. The results at the quasilinear time t_1 are mainly used to compare with the quasilinear theories, while the results at the nonlinear time t_2 are used to analyze the characteristics of the phase-space structure of the ion diffusion tensor in fully developed turbulence, which cannot be predictedby the quasilinear theories.

3.2. Poloidal structure of the ion diffusion tensor

The components of the phase-space ion diffusion tensor D^{rr} and D^{rK} are the functions of the phase-space coordinate $(r, \theta, \zeta, v_\parallel, \mu)$, and we first analyze the structure in the θ direction in this section. The radial calculation position is chosen as $r = 0.45a$, around where the turbulence intensity is the highest. The velocity is chosen as $(\bar{v}_\parallel = 1, \bar{v}_\perp = 0.3)$ and $(\bar{v}_\parallel = 0.3, \bar{v}_\perp = 1.4)$: the typical velocity of the passing ion and the trapped ion, respectively, where $\bar{v}_\parallel = v_\parallel/v_{\rm T}$, $\bar{v}_\perp = v_\perp/v_{\rm T}$, where $v_{\rm T}$ is the ion thermal velocity.

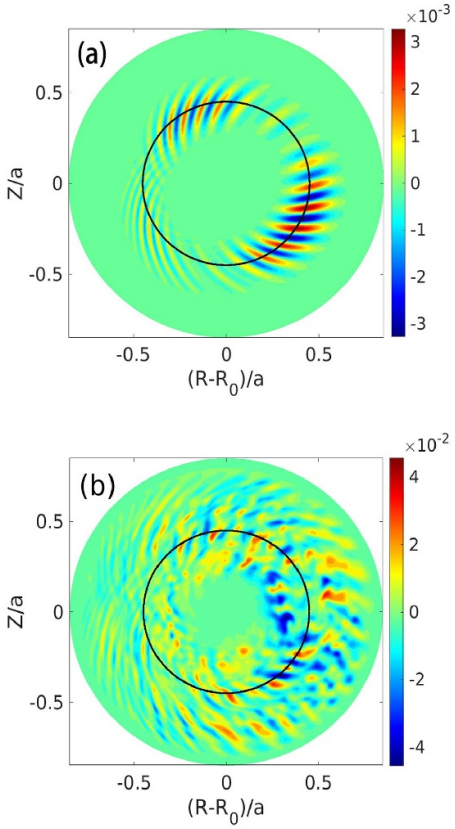

Figure 3. The mode structure of the fluctuating electrostatic potential of ITG turbulence, in which the magnetic surface of $r = 0.45a$ is labeled with a black line. (a) Linear stage (t_1); (b) nonlinear stage (t_2). $R = R_0 + r\cos\theta$, where θ is the poloidal coordinate.

The poloidal structures of D^{rr} and D^{rK} are shown in figure 4. At the quasilinear time t_1, D^{rr} and D^{rK} are approximately proportional to $(1 + \cos\theta)$, either for the passing ion or the trapped ion. At the nonlinear time t_2, the poloidal structures are similar. The results suggest that for nonlinear fully developed ITG turbulence, the ion diffusion, and therefore the transport, mainly occurs in the low field side, which confirms the strong ballooning approximation widely used in transport research [7, 8]. Note that the specific relation between the ion diffusion tensor and poloidal angle found here has not been pointed out in previous work.

3.3. Velocity space of the ion diffusion tensor

In this section, we analyze the structure of D^{rr} and D^{rK} in velocity space. The radial position and toroidal average are the same as those in the previous section. The poloidal position is chosen as $\theta = 0$, where the diffusion is the strongest. The D^{rr} and D^{rK} at 64×16 velocity grid points are calculated. The velocity-space structures of D^{rr} and D^{rK} are shown in figure 5. It can be seen that at quasilinear time t_1, D^{rr} and D^{rK} both present an elliptical band structure with the axial ratio close to $\sqrt{2}$; the ion diffusion tensor decreases gradually as

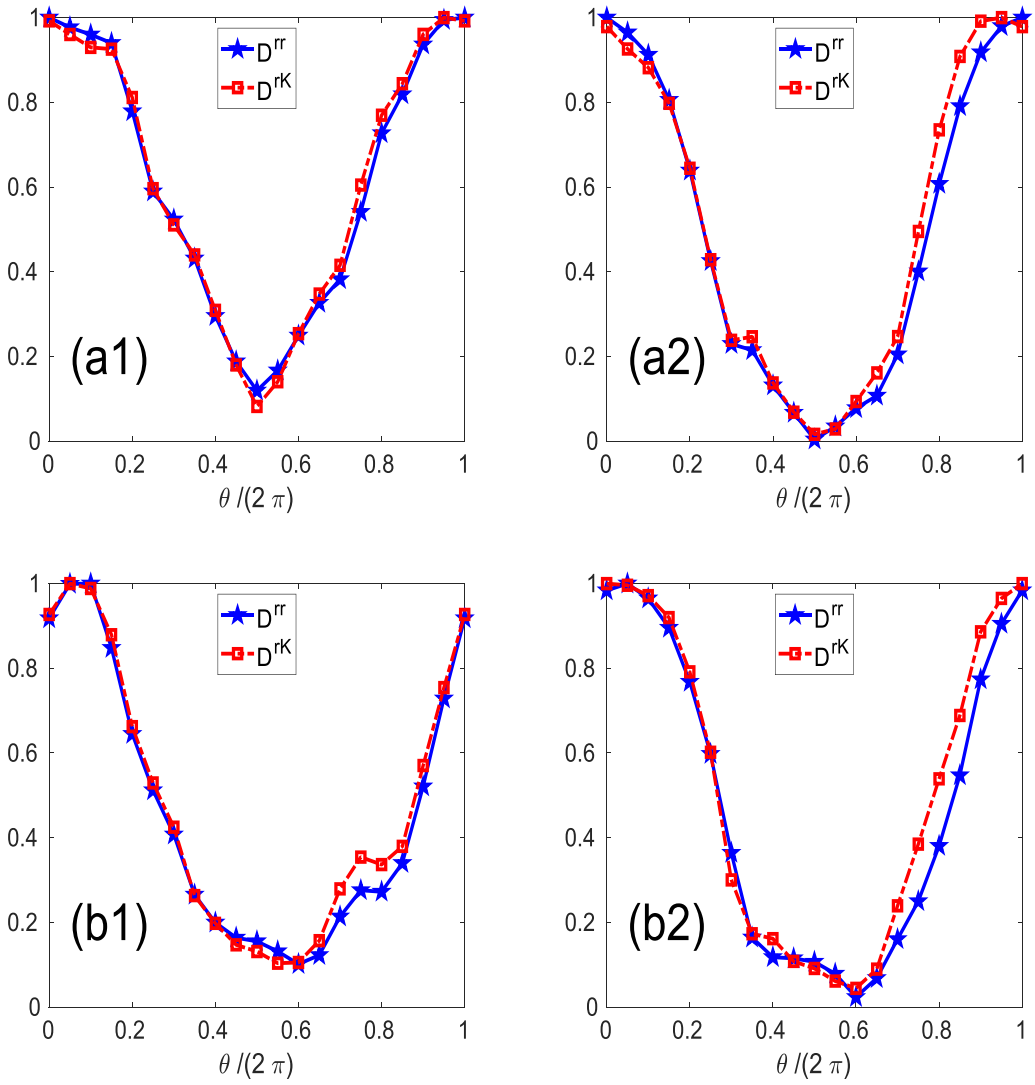

Figure 4. The poloidal structure of D^{rr} and D^{rK}: ($a1$) time t_1, $\bar{v}_{\|}=1$,$\bar{v}_{\perp}=0.3$; ($a2$) time t_1, $\bar{v}_{\|}=0.3$, $\bar{v}_{\perp}=1.4$; ($b1$) time t_2, $\bar{v}_{\|}=1$, $\bar{v}_{\perp}=0.3$; ($b2$) time t_2, $\bar{v}_{\|}=0.3$, $\bar{v}_{\perp}=1.4$. Here, D^{rr} (blue line) and D^{rK} (red line) are normalized by the maximum value in the poloidal direction.

the velocity points deviate from the center of the band. More importantly, the velocity-space structure at nonlinear time t_2 still retains similar properties. Note that the effects of both passing and trapped particles are considered in the simulation. The trapped–passing boundary is labeled in figure 5, and it can be seen that the contribution from trapped particles to diffusion is greater than that from passing particles.

The ion diffusion tensor of ITG turbulence calculated by quasilinear theory is given as [10]

$$D^{rr}=\sum_{nm}\frac{k_\theta^2}{B^2}|\delta\phi_{nm}|^2\frac{\gamma}{(\omega_r-\omega_d)^2+\gamma^2}, \tag{10a}$$

$$D^{rK}=\sum_{nm}-m_i\frac{v_{\|}^2+v_{\perp}^2/2}{R}\frac{k_\theta^2}{B^2}|\delta\phi_{nm}|^2\frac{\gamma}{(\omega_r-\omega_d)^2+\gamma^2}, \tag{10b}$$

in which $\omega_d=-k_\theta\frac{m_i(v_{\|}^2+v_{\perp}^2/2)}{e_sRB}$, $k_\theta=m/r$. Here, $\delta\phi_{nm}$ is the Fourier coefficient of the turbulent electrostatic potential, where m and n are the poloidal and toroidal Fourier mode numbers, respectively; ω_r and γ are the mode frequency and growth rate, respectively. Note that ω_r and γ is also a function of the mode number, and there we drop the symbols n and m for convenience. In equations (10a) and (10b), the $k_{\|}v_{\|}$ term ($k_{\|}=\frac{m-nq}{qR}$) is neglected. Note the fact that the contribution from trapped particles to the ion diffusion tensor is greater than that from passing particles, especially at the quasilinear time t_1, and the ion drift orbit width is larger than the width of the local mode (poloidal harmonics); when the particles cross the rational surface, the sign of $v_{\|}$ does not change, but that of $k_{\|}$ changes. Therefore, it is not hard to understand that the $k_{\|}v_{\|}$ term will be canceled when computing the ion diffusion tensor over an ensemble-average time (2∼3 bounce period), which can also be verified from figure 5 in that the shift of the

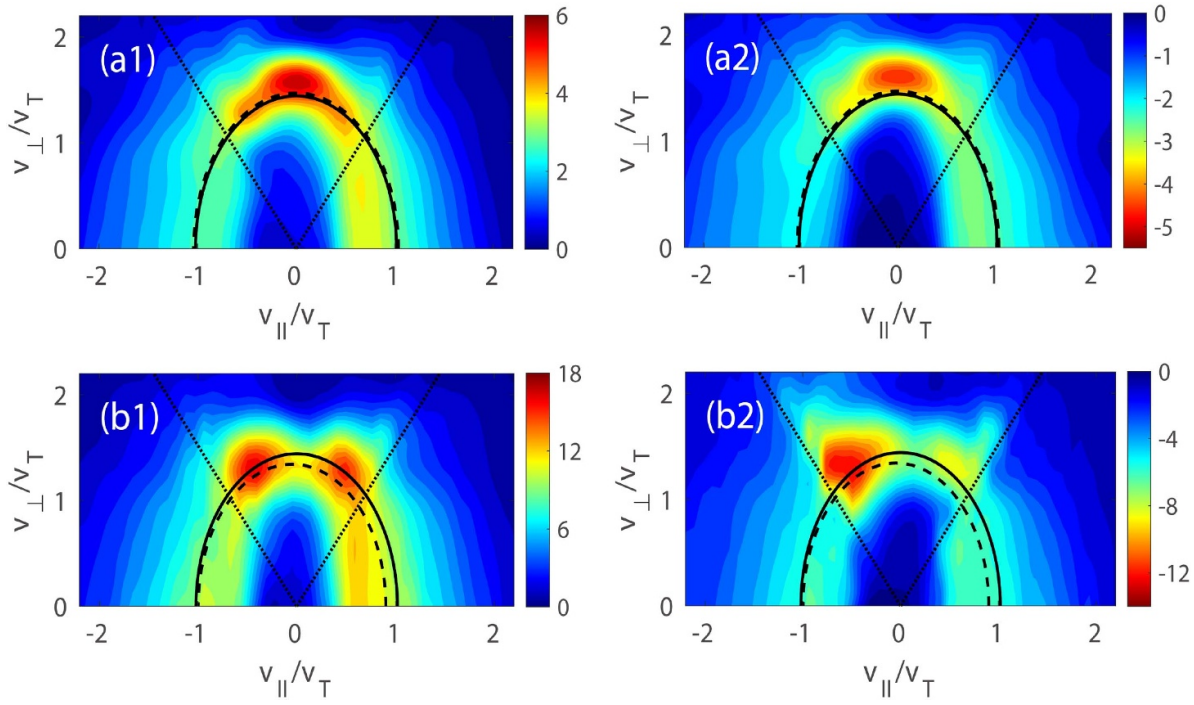

Figure 5. The velocity-space structure of D^{rr} and D^{rK}: ($a1$) D^{rr} at time t_1; ($a2$) D^{rK} at time t_1; ($b1$) D^{rr} at time t_2; ($b2$) D^{rK} at time t_2. Here, D^{rK} is normalized by $T_{\rm ref}/a$. The solid line is the quasilinear resonance line, the dashed line is the fitting center line, and the dotted lines are the passing and trapped particles' velocity-space boundary lines.

resonance structure of D^{rr} and D^{rK} in the $v_\parallel$ direction is small enough.

An ITG eigenmode has a definite toroidal mode number due to the toroidicity-induced coupling effect; meanwhile, poloidal harmonics with the same n but different m are localized on their corresponding rational surface r_m, with $q(r_m) = m/n$. Thus, equation (10a) can be written as [10]

$$\begin{aligned} D^{rr} &\approx \sum_n \frac{k_\theta^2}{B^2}|\delta\phi_n|^2 \frac{\gamma}{(\omega_r-\omega_d)^2+\gamma^2} \\ &\approx \sum_n D_n \delta(\bar{v}_\parallel^2 + \bar{v}_\perp^2/2 - \omega_r/\omega_{0n}), \end{aligned} \tag{11}$$

with $D_n = \frac{\pi n^2 q^2}{r^2 B^2}\frac{|\delta\phi_n|^2}{|\omega_{0n}|}$, $\omega_{0n} = -\frac{2nqT_0}{erBR}$. Note that in equation (11), we have used the approximation that the growth rate is much less than the mode frequency. Here, ω_r should be understood as the linear eigen frequency.

By further considering the fact that the diffusion in the linear stage is mainly contributed by the mode with the greatest growth rate, we can obtain the equation of the quasilinear resonance line

$$D^{rr} = D_n \delta(\bar{v}_\parallel^2 + \bar{v}_\perp^2/2 - \omega_r/\omega_{0n}), \tag{12a}$$

$$D^{rK} = -m_i \frac{v_\parallel^2 + v_\perp^2/2}{R} D_n \delta(\bar{v}_\parallel^2 + \bar{v}_\perp^2/2 - \omega_r/\omega_{0n}), \tag{12b}$$

Here, n should be chosen as the mode number of the Fourier mode with the greatest growth rate, which can be found through linear ITG simulations under the same equilibrium using the NLT code. In the linear ITG simulations, the frequency and growth rate of each Fourier mode (local modes) are calculated by

$$\omega_r(t) \equiv \frac{\rm d}{{\rm d}t}\Im\{\ln[\delta\phi_{nm}(r_m,t)]\}, \tag{13a}$$

$$\gamma(t) \equiv \frac{\rm d}{{\rm d}t}\Re\{\ln[\delta\phi_{nm}(r_m,t)]\}. \tag{13b}$$

It is found that the $n = 20$ eigenmode has the greatest growth rate; therefore, the quasilinear resonance line in equation (12a) or equation (12b) is calculated with the eigenmode frequency $n = 20$, as shown in figure 5. The center line of the numerical results can be obtained by data fitting

$$D^{rr}(\bar{v}_\parallel, \bar{v}_\perp) = D_0 \exp\left(-\frac{(\bar{v}_\parallel + a_1)^2 + \frac{1}{2}\bar{v}_\perp^2 - a_2}{\lambda^2}\right), \tag{14}$$

which is also shown in figure 5. It can be seen that the fitting center line at the linear stage agrees well with the quasilinear resonance line, and the fitting center line at the nonlinear stage deviates slightly from the quasilinear resonance line.

Compared with the quasilinear resonance line, the numerical results present a band structure with finite width that is obviously larger than the interval of the velocity-space grid ($\Delta\bar{v}_\parallel \approx 0.1$, $\Delta\bar{v}_\perp \approx 0.3$) or the broadening width induced by mode growth, which may refer to the famous nonlinear resonance broadening [24]. However, the broadening width at t_2 is close to that at t_1, even though the turbulence amplitude at t_2 is much larger than that at t_1; this is different from the prediction of the previous nonlinear theory [25]. The numerical results

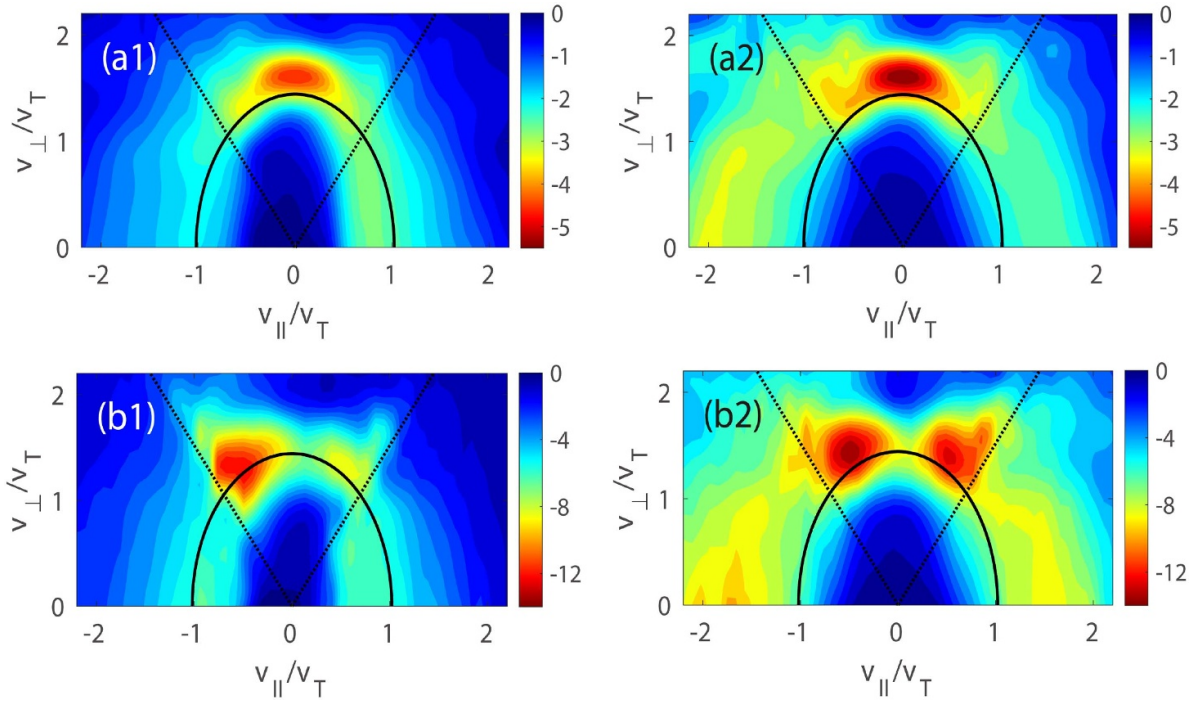

Figure 6. The Stokes–Einstein relation. The numerical results of D^{rK} at time t_1 and time t_2 are shown in ($a1$) and ($b1$), respectively; D^{rK} obtained from the numerical results of D^{rr} using the Stokes–Einstein relation at time t_1 and time t_2 is shown in ($a2$) and ($b2$), respectively. The solid line is the quasilinear resonance line, and the dotted lines are the passing and trapped particles' velocity-space boundary lines.

imply that the nonlinear resonance broadening in toroidal ITG turbulence may not be mainly induced by the stochastic turbulent scattering, but other orbit effects, such as the variation of poloidal drift velocity.

3.4. The relation between D^{rr} and D^{rK}

It can be seen from the results in the previous subsections that the D^{rr} and D^{rK} present similar phase-space structures at the linear stage. It is further found that D^{rr} and D^{rK} at the linear stage satisfy the famous Stokes–Einstein relation

$$D^{rK} = -m_i \frac{v_{\|}^2 + v_{\perp}^2/2}{R} D^{rr}, \tag{15}$$

as shown in figures 6($a1$) and ($a2$). It has been proven that equation (15) also works at the nonlinear stage [26]. It is found that D^{rr} and D^{rK} at the nonlinear stage roughly satisfy equation (15), as shown in figures 6($b1$) and ($b2$). The velocity-space passing–trapping boundary line is labeled in figure 6. It can be seen from figure 6 that D^{rK} is mainly contributed by trapped particles and, in the trapping cone, the D^{rK} directly obtained by NDTM is close to that obtained using equation (15), which indicates equation (15) is well satisfied; meanwhile, out of the trapping cone, especially in the velocity space of $v_{\perp} < v_T$ outside of the resonance curve, a difference is found between D^{rK} obtained by the above two methods, which indicates equation (15) is not well satisfied. The reasons for the difference are as follows: (1) note that in obtaining equation (15) [26], the $\cos\theta \approx 1$ was used by invoking the strong ballooning approximation; when the strong ballooning approximation is not well satisfied, $\cos\theta \approx 1$ is still a good approximation for trapped particles, but not a good one for passing particles; (2) the coefficient, $m_i \frac{v_{\|}^2 + v_{\perp}^2/2}{R}$, in equation (15) has an amplification effect on the error of D^{rr}. The more outside of the resonance curve, the larger the coefficient, $m_i \frac{v_{\|}^2 + v_{\perp}^2/2}{R}$, and the larger the difference between the D^{rK} directly obtained by the NDTM and the D^{rK} obtained using equation (15).

4. The resonance structures of the ion diffusion tensor in single-*n* modes and the superposition effect of multiple n modes

According to equation (11), when the ion magnetic drift frequency and the frequency of a linear ITG eigenmode satisfy the relation

$$\omega_d \approx \omega_r, \tag{16}$$

the ion will resonate with the single-n modes and thus induce diffusion; the total ion diffusion tensor is the linear superposition of ion diffusion tensors contributed by all single-n modes. However, when the turbulence is saturated, the frequencies of single-n ITG modes are changed under the influence of nonlinear effects; it is not clear how the ion would resonate with these nonlinear single-n modes and whether the linear superposition property still remains. In this section, we will analyze the structure of ion diffusion tensors in single-n modes and the superposition of multiple modes to further understand

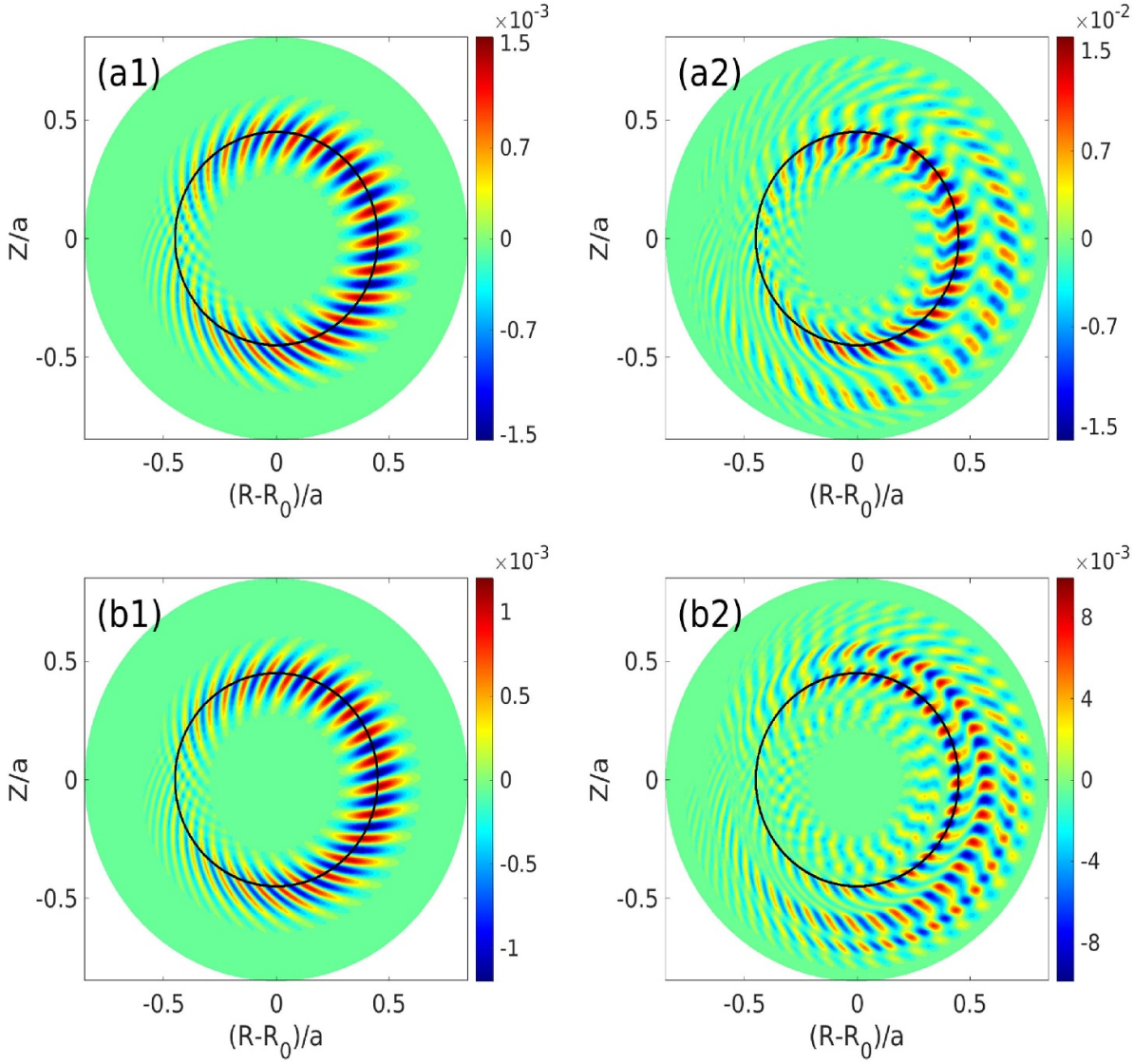

Figure 7. The mode structures of fluctuating electrostatic potentials of single-n toroidal modes, in which the magnetic surface of $r = 0.45a$ is labeled with a black line. ($a1$) Mode $n = 20$ at time t_1; ($a2$) mode $n = 20$ at time t_2; ($b1$) mode $n = 22$ at time t_1; ($b2$) mode $n = 22$ at time t_2.

the previous numerical results. The toroidal modes $n = 20$ and $n = 22$ are chosen for analysis; the two modes make the most important contribution to the turbulent transport at both time t_1 and time t_2, as shown in figure 2. The mode structures of $n = 20$ and $n = 22$ are shown in figure 7.

For the quasilinear time t_1, we firstly compute the ion diffusion tensor in the superposition field of the toroidal modes $n = 20$ and $n = 22$ using the NDTM code, as shown in figure 8. The quasilinear resonance line calculated by equation (16), with ω_r taken as the linear eigenmode frequency, is labeled in figure 8. Note that the quasilinear resonance lines plotted in figures 5 and 6 were calculated in the same way. It can be seen by comparing figure 8 with figure 5($a1$) that both ion diffusion tensors present elliptical band structures with the axial ratio close to $\sqrt{2}$, and both band structures are close to the quasilinear resonance line; this indicates that the velocity-space structure of the ion diffusion tensor in the superposition field of toroidal modes $n = 20$ and $n = 22$ presents a resonant structure very similar to that found in the total turbulence field. Moreover, the ion diffusion tensor in the superposition field of toroidal modes $n = 20$ and $n = 22$ contributes more than 80% of the ion diffusion tensor in the total turbulence field, which indicates that the ion diffusion tensor in the total turbulence field at t_1 is mainly contributed by the superposition field of toroidal modes $n = 20$ and $n = 22$.

Then, we compute the ion diffusion tensors in the single toroidal modes $n = 20$ and $n = 22$, respectively, and sum these two ion diffusion tensors together, as shown in figures 9($a1$), ($a2$) and (b). The quasilinear resonance lines calculated by equation (16), with ω_r taken as the linear eigenmode frequency, are labeled in all the panels of figure 9. It can be seen by comparing figures 9($a1$) and ($a2$) with figure 8, respectively, that both ion diffusion tensors present similar band structures, and both band structures are close to the quasilinear resonance line; this indicates that the velocity-space structure of the ion diffusion tensor in both single toroidal modes

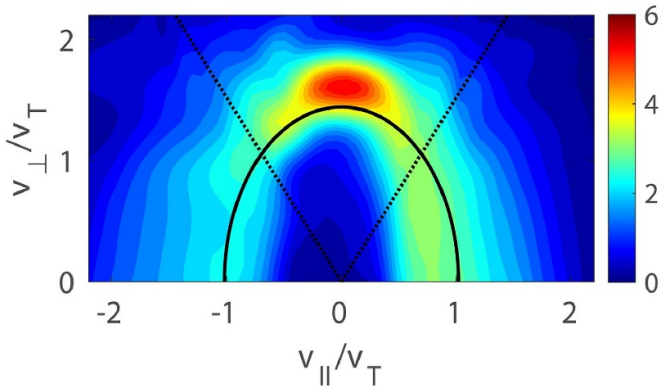

Figure 8. The D^{rr} in the superposition field of toroidal modes $n=20$ and $n=22$ (t_1). The solid line is the quasilinear resonance line calculated by equation (16), with ω_r taken as the linear eigenmode frequency, and the dotted lines are the passing and trapped particles' velocity-space boundary lines.

$n=20$ and $n=22$ present a resonant structure very similar to that found in the superposition field of toroidal modes $n=20$ and $n=22$, which can be well understood by equation (16). Moreover, it can be found that the sum of ion diffusion tensors in toroidal modes $n=20$ and $n=22$ is close to the ion diffusion tensor in the superposition field of toroidal modes $n=20$ and $n=22$ by comparing figure 9(b) with figure 8. Therefore, the phase-space structure of the ion diffusion tensor in the total turbulence field at the quasilinear time t_1 can be understood as the result of resonance between the ion and single-n toroidal modes through the linear resonance relation equation (16).

For the nonlinear time t_2, it is found that the $n=0$ mode (mainly zonal flows), which can be neglected at the linear stage, grows significantly after saturation (as shown in figure 10). We firstly compute the ion diffusion tensor in the superposition field of toroidal modes $n=20+22$ and $n=0+20+22$ using the NDTM code, respectively, as shown in figures 11(a) and (b). The quasilinear resonance lines calculated by equation (16), with ω_r taken as the linear eigenmode frequency, are labeled in all the panels of figure 11. Note that, for time t_2, the quasilinear resonance line calculated by equation (16), with ω_r taken as the linear eigenmode frequency, is only a reference line to make a comparison between the ion diffusion tensors. It can be seen by comparing figure 11(a) with figure 11(b) that both the velocity-space structure and the value of D^{rr} are different between the superposition field of toroidal modes $n=20+22$ and $n=0+20+22$. For the ion diffusion tensor in the superposition field of toroidal modes $n=0+20+22$, it can be seen by comparing figure 11(b) with figure 5($b1$) that both ion diffusion tensors present similar band structures, and both band structures are close to the quasilinear resonance line, which indicates the velocity-space structure of the ion diffusion tensor in the superposition field of toroidal modes $n=0+20+22$ presents a resonant structure very similar to that found in the total turbulence field. Moreover, the ion diffusion tensor in the superposition field of toroidal modes $n=0+20+22$ contributes 60% of that in the total turbulence field, which indicates that zonal flows and several toroidal ITG modes with large

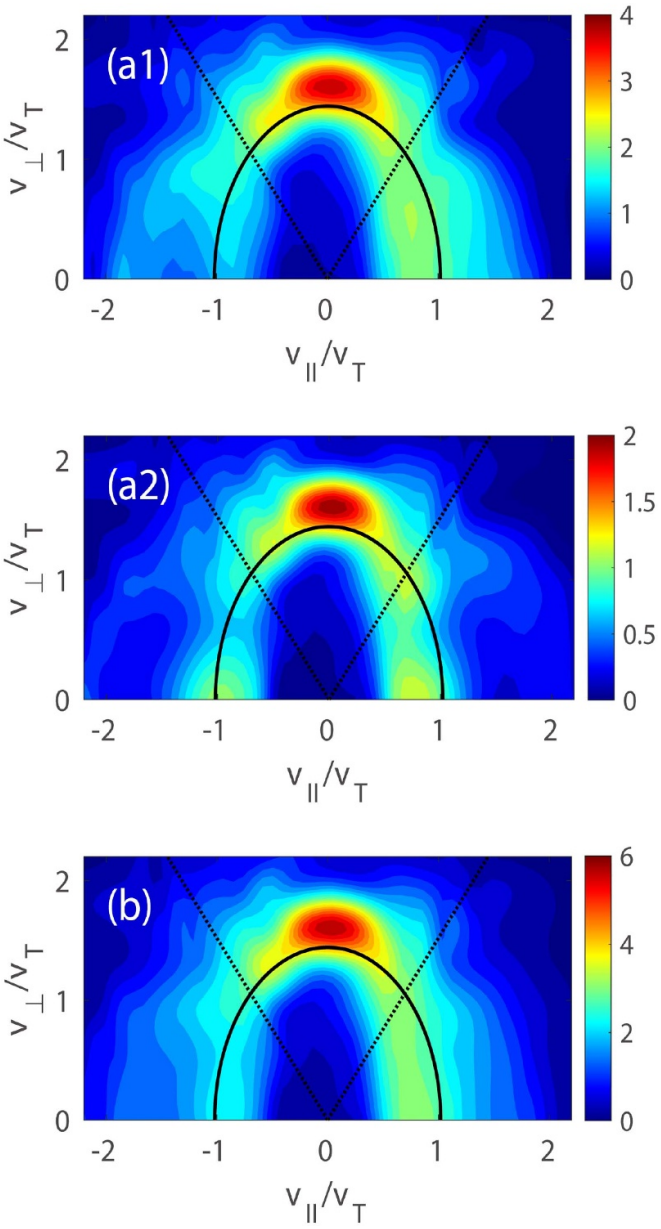

Figure 9. The D^{rr} in different toroidal modes (t_1). ($a1$) Mode $n=20$; ($a2$) mode $n=22$; (b) the sum of D^{rr} in toroidal modes $n=20$ and $n=22$. The solid line is the quasilinear resonance line calculated by equation (16), with ω_r taken as the linear eigenmode frequency, and the dotted lines are the passing and trapped particles' velocity-space boundary lines.

amplitude contribute quite importantly to the anomalous transport at the nonlinear stage.

Then, we compute the ion diffusion tensors in the superposition field of toroidal modes $n=0+20$ and $n=0+22$, respectively, and sum these two ion diffusion tensors together, as shown in figures 12($a1$), ($a2$) and (b). The quasilinear resonance lines calculated by equation (16), with ω_r taken as the linear eigenmode frequency, are labeled in all the panels of figure 12. It can be seen by comparing figure 12(b) with figure 11(b) that both ion diffusion tensors present similar band structures, both band structures are close to the quasilinear resonance line, and the values of both ion diffusion

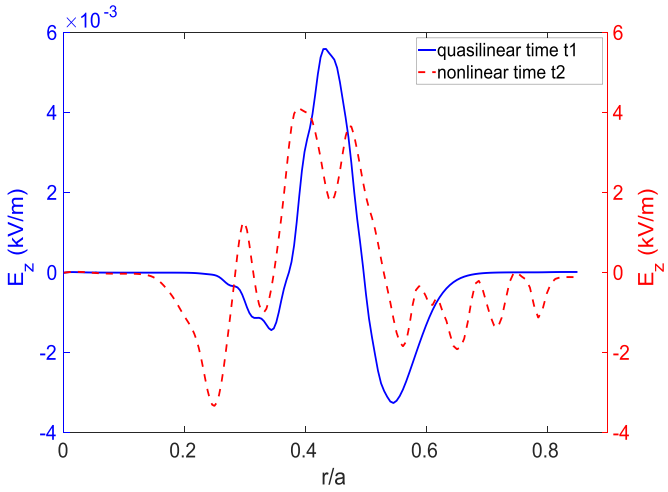

Figure 10. The radial structure of the fluctuating electrostatic potential of $n=0$ mode. The solid line in blue represents the quasilinear time t_1, and the dashed line in red represents the nonlinear time t_2.

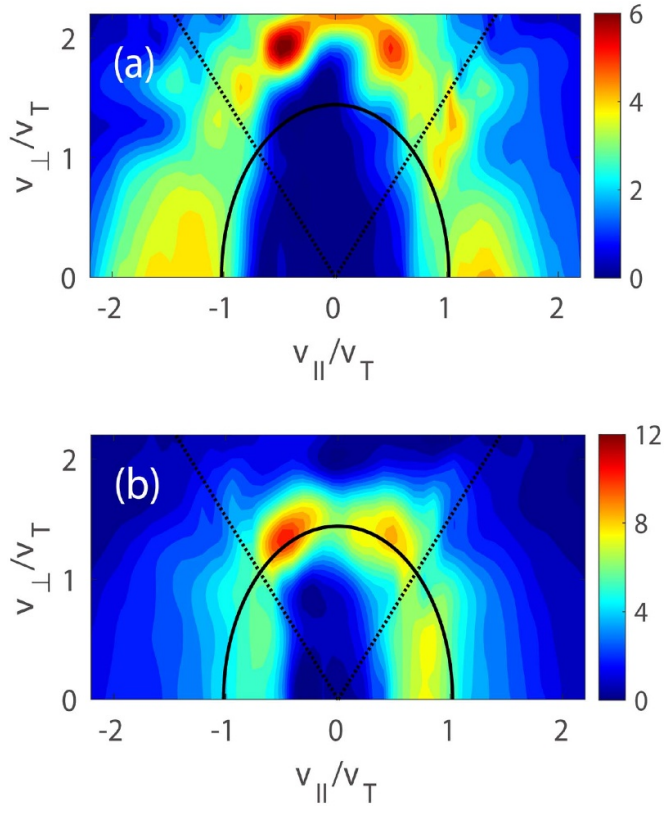

Figure 11. The D^{rr} in the superposition field of toroidal modes (t_2). (a) Mode $n=20+22$, (b) mode $n=0+20+22$. The solid line is the quasilinear resonance line calculated by equation (16), with ω_r taken as the linear eigenmode frequency, and the dotted lines are the passing and trapped particles' velocity-space boundary lines.

tensors are similar; this indicates that the sum of the ion diffusion tensors in the superposition field of toroidal modes $n=0+20$ and $n=0+22$ is close to the ion diffusion tensor in the superposition field of toroidal modes $n=0+20+22$. Therefore, the ion diffusion tensor in the total turbulence field

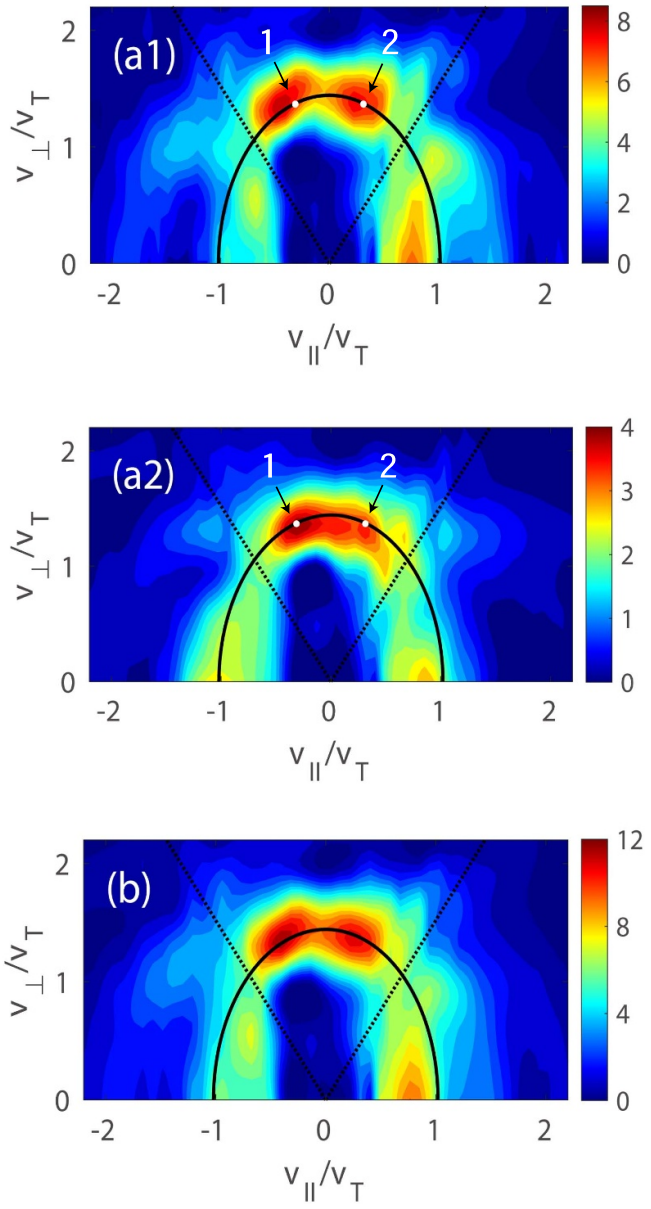

Figure 12. The D^{rr} in the superposition field of toroidal modes (t_2). ($a1$) Mode $n=0+20$; ($a2$) mode $n=0+22$; (b) the sum of D^{rr} in the superposition field of toroidal modes $n=0+20$ and $n=0+22$. The dotted lines are the passing and trapped particles' velocity-space boundary lines. The solid lines in ($a1$), ($a2$), and (b) are the quasilinear resonance lines calculated by equation (16), with ω_r taken as the linear eigenmode frequency. The text '1' and '2' in ($a1$) and ($a2$) represents the trapped particles selected.

at the nonlinear time t_2 is mainly contributed by the two most unstable toroidal modes $n=20$ and $n=22$ under the influence of zonal flows.

Note that the quasilinear resonance line shown in figures 12($a1$) and ($a2$) is calculated with ω_r taken as the linear eigenmode mode frequency; it is found from frequency analysis that around time t_2, the single-n eigenmodes are radially restructured into multiple daughter ballooning modes (DBMs) with time-variant frequency [27]; the DBM frequencies at time t_2 are shown in table 1. It is found that the

Table 1. The calculation results of ω_d and $\overline{\omega}_E$ at time t_2.

Field	ω_r ($/10^5$ Hz)	Particle	ω_d ($/10^5$ Hz)	$\omega_d+\overline{\omega}_E$ ($/10^5$ Hz)
$n=0+20$[a]	2.78	1	1.22	2.70
		2	1.22	2.70
$n=0+22$[a]	2.80	1	1.34	2.97
		2	1.34	2.97

[a] $n=0+20$ and $n=0+22$ represent the fact that the particles are in the superposition field of toroidal modes $n=0+20$ and $n=0+22$, respectively. Note that the linear eigenmode frequency is $\omega_r/10^5$ Hz $=1.21(1.33)$ for $n=20(22)$.

nonlinear resonance structures can be understood as the result of resonance between ions and DBMs through the nonlinear resonance relation [27]

$$\omega_d+\overline{\omega}_E\approx\omega_r, \tag{17}$$

where ω_r is the frequency of the DBM at the nonlinear stage;

$$\overline{\omega}_E=k_\theta\frac{\overline{E}_z}{B}, \tag{18}$$

where $E_z=-\partial_r\phi_{n=0,m=0}$ is the zonal radial electric field (REF). The orbit average operator is given by

$$\overline{E}_z=\frac{1}{\tau_p}\oint \mathrm{d}t' E_z[r(t')], \tag{19}$$

where E_z is integrated over a poloidal period along the particle orbit, and τ_p is the poloidal (bounce/transit) period (for trapped/passing particles). Compared with the linear resonance relation, the orbit-averaged poloidal acceleration induced by the zonal REF is considered in the nonlinear resonance relation.

Due to the fact that the contribution from trapped particles to diffusion is more important, two trapped particles are selected, as shown in figures 12(a1) and (a2), to compute ω_d and $\overline{\omega}_E$ at time t_2; the results are shown in table 1. It is found that ω_d does not agree with ω_r, while the sum of ω_d and $\overline{\omega}_E$ agrees well with ω_r for both two particles in the two cases with $n=0+20$ and $n=0+22$; this verifies the nonlinear resonance relation and indicates the importance of zonal flow at the nonlinear stage.

The nonlinear resonance structure shown in figures 12(a1) and (a2) is similar to the quasilinear resonance structure shown in figure 9; this can be understood as follows. The DBMs nonlinearly stem from the linear eigenmode [27], and the modes are resonantly excited; since the energy of the resonant particle does not change much from the linear to the nonlinear stage, the phase-space resonance structure does not change much from the linear to the nonlinear stage. However, from the linear to the nonlinear stage, the resonant particles are poloidally accelerated by the nonlinearly excited zonal REF; therefore, the mode frequency is nonlinearly shifted up. This explains the nonlinear frequency chirping of the mode [27].

5. Summary and discussion

In conclusion, in a typical ITG turbulence simulated by the NLT code under Cbc test parameters, the ion phase-space diffusion tensor is computed using the numerical diagnosis code NDTM.

The numerical results show that at both the linear stage and the nonlinear fully saturated stage of the turbulence, the ion diffusion tensor presents similar structural properties: in the poloidal direction, the ion diffusion tensor is approximately proportional to $(1+\cos\theta)$; in velocity space, the diffusion tensor presents a magnetic drift resonance structure with finite broadening; the D^{rr} and D^{rK} components of the ion diffusion tensor satisfy the Stokes–Einstein relation.

To further understand the numerical results, the diffusion tensor in single-n toroidal modes is studied. It is found that at both the linear and the nonlinear stages, the total ion diffusion tensor is approximately the sum of the diffusion tensor contributed by single-n modes. At the linear stage, the diffusion in single-n modes is induced by the resonance between ions and ITG eigenmodes; while at the nonlinear stage, the diffusion in single-n modes is induced by the resonance between ions and DBMs under the poloidal acceleration of the zonal REF. Although the resonance mechanisms are different, the induced resonance structures are similar, which leads to the similarity between the phase-space structures of ion diffusion tensors at the linear and nonlinear stages of ITG turbulence.

Acknowledgments

This work was supported by the National Natural Science Foundation of China under Grant Nos. 12075240 and 11875254, and the National MCF Energy R&D Program of China No. 2019YFE03060000.

ORCID iDs

Shiqiao Sun https://orcid.org/0000-0002-5900-7034
Yuesong Li https://orcid.org/0000-0002-7102-3678
Zihao Wang https://orcid.org/0000-0001-5545-4411
Shaojie Wang https://orcid.org/0000-0002-2786-519X

References

[1] Balescu R. 2005 *Aspects of Anomalous Transport in Plasmas* (IOP Publishing)

[2] Braginskii S.I. 1965 Transport Processes in a Plasma *Reviews of Plasma Physics* vol 1 ed M.A. Leontovich (Consultants Bureau) p 205
[3] Galeev A.A. and Sagdeev R.Z. 1968 *Sov. Phys.-JETP* **26** 233
[4] Gary S.P. 1993 *Theory of Space Plasma Microinstabilities* (*Cambridge Atmospheric and Space Science Series*) (Cambridge University Press)
[5] Escande D.F. and Sattin F. 2007 *Phys. Rev. Lett.* **99** 185005
[6] Wang S. 2012 *Phys. Plasmas* **19** 062504
[7] Peeters A.G., Angioni C. and Strintzi D. 2007 *Phys. Rev. Lett.* **98** 265003
[8] Hahm T.S., Diamond P.H., Gurcan O.D. and Rewoldt G. 2008 *Phys. Plasmas* **15** 055902
[9] Eriksson L.G., Righi E. and Zastrow K.D. 1997 *Plasma Phys. Control. Fusion* **39** 27
[10] Zhang D., Xu Y. and Wang S. 2017 *Phys. Plasmas* **24** 030701
[11] Levinton F.M. *et al* 1995 *Phys. Rev. Lett.* **75** 4417
[12] Fujita T., Ide S., Shirai H., Kikuchi M., Naito O., Koide Y., Takeji S., Kubo H. and Ishida S. 1997 *Phys. Rev. Lett.* **78** 4529
[13] Bernstein I.B. and Engelmann F. 1966 *Phys. Fluids* **9** 937–52
[14] Horton W., Choi D.I. and Tang W.M. 1981 *Phys. Fluids* **24** 1077
[15] Artaud J.F. *et al* 2010 *Nucl. Fusion* **50** 043001
[16] Diamond P.H., Itoh S.I. and Itoh K. 2010 *Physical Kinetics of Turbulent Plasmas* (*Cambridge Atmospheric and Space Science Series*) (Cambridge University Press)
[17] Wang S. 2016 *Phys. Plasmas* **23** 022303
[18] Sun S., Zhu S., Dai Z. and Wang S. 2021 *Phys. Plasmas* **28** 052301
[19] Wang S. 2013 *Phys. Plasmas* **20** 082312
[20] Xu Y., Ye L., Dai Z., Xiao X. and Wang S. 2017 *Phys. Plasmas* **24** 082515
[21] Dai Z., Xu Y., Ye L., Xiao X. and Wang S. 2019 *Comput. Phys. Commun.* **242** 72
[22] Ye L., Xu Y., Xiao X., Dai Z. and Wang S. 2016 *J. Comput. Phys.* **316** 180
[23] Dimits A.M. *et al* 2000 *Phys. Plasmas* **7** 969
[24] Dupree T.H. 1966 *Phys. Fluids* **9** 1773
[25] Dupree T.H. 1967 *Phys. Fluids* **10** 1049
[26] Wang S. 2016 *Phys. Plasmas* **23** 072509
[27] Sun S., Wang Z., Wang S. and Dai Z. 2022 *Nucl. Fusion* **62** 126005